Accepted refereed manuscript of:

Varley A, Tyler A, Bondar Y, Hosseini A, Zabrotski V & Dowdall M (2018) Reconstructing the deposition environment and long-term fate of Chernobyl (137)Cs at the floodplain scale through mobile gamma spectrometry, *Environmental Pollution*, 240, pp. 191-199.

DOI: 10.1016/j.envpol.2018.04.112

Title: Reconstructing the deposition environment and long-term fate of Chernobyl ^{137}Cs at the floodplain scale through mobile gamma spectrometry.

Authors: Adam Varley[1], Andrew Tyler[1], Yuri Bondar[2], Ali Hosseini[3], Viachaslau Zabrotski[2] and Mark Dowdall[3].

Affiliations:

[1]Department of Biological and Environmental Sciences, University of Stirling, Stirling FK9 4LA, United Kingdom

[2]Norwegian Radiation Protection Authority, Grini næringspark 13, 1332 Østerås, Norway

[3]Polessie State Radiation-Ecological Reserve, Tereshkovoy Street 7, Khoiniki, Gomel Region, Belarus

Keywords: Caesium redistribution; Sedimentation rates; Floodplain functioning; Gamma-ray spectrometry; Chernobyl

Abstract:

Cs-137 is considered to be the most significant anthropogenic contributor to human dose and presents a particularly difficult remediation challenge after a dispersal following nuclear incident. The Chernobyl Nuclear Power Plant meltdown in April 1986 represents the largest nuclear accident in history and released over 80 PBq of ^{137}Cs into the environment. As a result, much of the land in close proximity to Chernobyl, which includes the Polessie State Radioecology Reserve in Belarus, remains highly contaminated with ^{137}Cs to such an extent they remain uninhabitable. Whilst there is a broad scale understanding of the depositional patterns within and beyond the exclusion zone, detailed mapping of the distribution is often limited. New developments in mobile gamma spectrometry provide the opportunity to map the fallout of ^{137}Cs and begin to reconstruct the depositional environment and the long-term behaviour of ^{137}Cs in the environment. Here, full gamma spectrum analysis using algorithms based on the peak-valley ratio derived from Monte Carlo simulations are used to estimate the total ^{137}Cs deposition and its depth distribution in the soil. The results revealed a pattern of ^{137}Cs distribution consistent with the deposition occurring at a time of flooding, which is validated by review of satellite imagery acquired at similar times of the year. The results were also consistent with systematic burial of the fallout ^{137}Cs by annual flooding events. These

results were validated by sediment cores collected along a transect across the flood plain. The true merit of the approach was confirmed by exposing new insights into the spatial distribution and long term fate of ^{137}Cs across the floodplain. Such systematic patterns of behaviour are likely to be fundamental to the understanding of the radioecological behaviour of ^{137}Cs whilst also providing a tracer for quantifying the ecological controls on sediment movement and deposition at a landscape scale.

Research capsule:

Complex deposition patterns of ^{137}Cs have been observed on floodplains providing insight into the role environmental processes play in the spatio-temporal redistribution of contamination

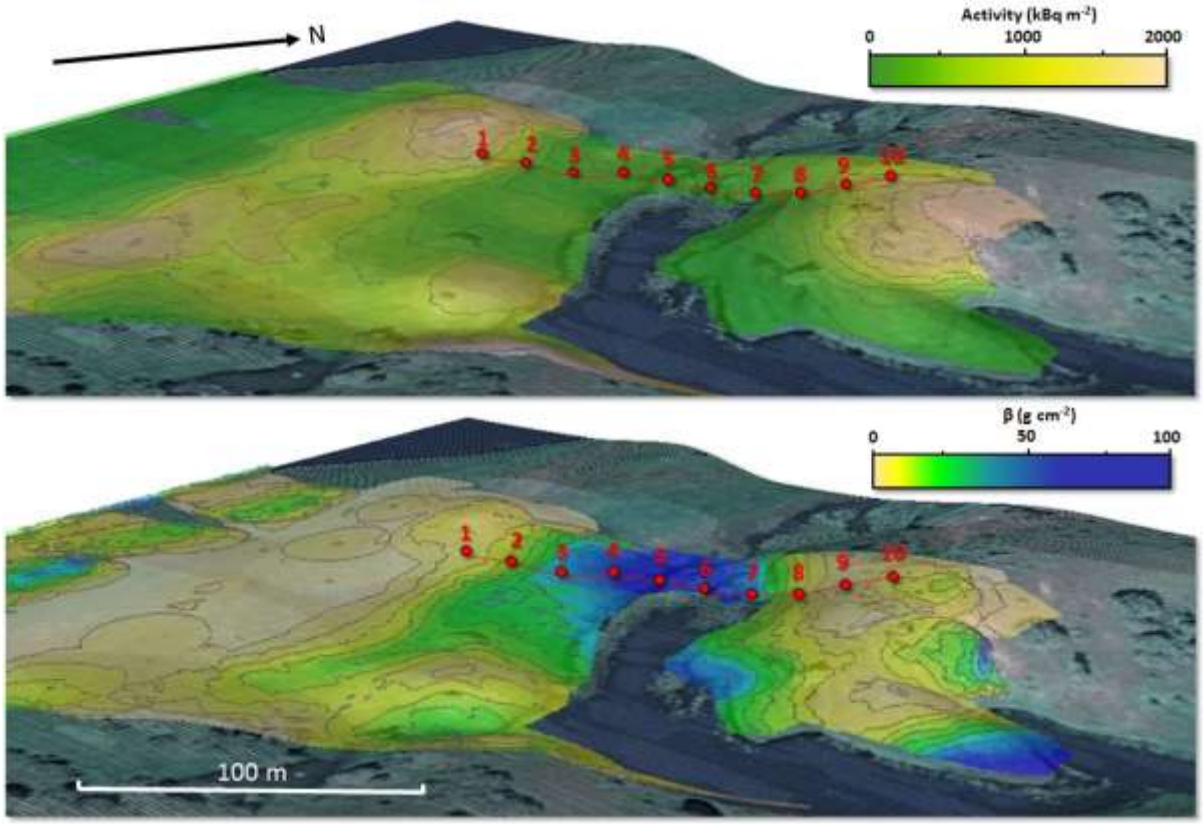

Graphical abstract. Interpolated handheld gamma-ray spectrometry estimates for activity (kBq $m^{=2}$) and β (g cm^{-2})

1. Introduction

Cs-137 is considered the one of the most radiologically significant anthropogenic radionuclide within the environment (Miller, 2007). The majority of present day global inventory of ^{137}Cs is derived from atmospheric weapons testing (1945-1963). More recently, further more-localised contamination has been introduced into the environment through reactor meltdowns occurring at Chernobyl Nuclear Power Plant (ChNPP) in 1986 and Fukishima Diachii Nuclear Power Plant (FDNPP) in 2011. The widespread nature of ^{137}Cs and the risk it poses to human health are as a result of a combination of physical and chemical properties. Foremost, it is one of the more abundant fission products generated during a nuclear chain reaction and it has a relatively low melting point (670.8 °C) allowing it to readily disperse into the atmosphere after a meltdown or nuclear bomb detonation (Isaksson and Raaf, 2017). Once in the environment, it can exhibit complex biogeochemical behaviour given it is highly soluble, has a tendency to react with environmental media in particular clay minerals and can be readily mobilised in the presence of organic matter. It can also easily enter the food chain as it is readily taken up into plant material substituting for naturally occurring potassium (Penrose et al., 2016). In terms of human exposure, the combination of 30.1 year half-life, high energy beta decay and the 662 keV gamma-ray from the short-lived daughter product ^{137m}Ba make ^{137}Cs both an internal and external radiation hazard. As a result, following any nuclear incident one of the fundamental tasks is to establish, using high quality data, the extent and intensity of ^{137}Cs deposition to inform decision making. This need has been exemplified by, for example, the largescale data collection efforts initiated by the Ministry of Education, Culture, Sports, Science and Technology (MEXT) within a month of the FDNPP accident (Povinec et al., 2013) and the multinational efforts over a number of decades to confidently characterise the spatial distribution of fallout across Europe after the ChNPP accident (Izrael et al., 1996).

In the longer term, continued measurement of ^{137}Cs is also important, not only to update population dose assessments (Beresford et al., 2016; Konoplev et al., 2017), but to monitor redistribution of the radiocontaminant within the environment occurring as a function soil movement, weathering and erosion (Rawlins et al., 2011). These are the same process that have enabled soil scientists to regularly utilise ^{137}Cs as a medium-term tracer for soil redistribution since the 1960's (Mabit and Dercon, 2014; Ritchie and McHenry, 1990).

Cs-137 is relatively straightforward to measure through gamma-ray spectrometry of the 662 keV photon released by its daughter product ^{137m}Ba within which it is always in secular equilibrium (Povinec et al., 2003). However, difficulties often arise when trying to account for depth variation of ^{137}Cs contamination given that significant penetration into the soil column can occur over time making precise estimates of the total inventory (Bq m^2) problematic (Tyler, 2004). The oldest and most direct way to measure the depth distribution is by extracting cores from a site and measuring small increments of the core (typically less than 5 cm slices) within the laboratory using low background High Purity Germanium (HPGe) detectors; thus building a profile. Collection, preparation and analysis of environmental samples can nonetheless make this procedure time consuming and expensive often yielding limited spatial representivity, which can become a major issue when significant spatial heterogeneity of contamination is encountered (Golosov et al., 2000). Possibly a more appropriate method that can address spatial resolution issues more effectively is the deployment of field-based mobile gamma-ray spectrometry (Tyler, 2008). Utilising this technique, measurements can be made directly in the field using a variety of gamma-ray detectors mounted to a specific platform such as static surveyor stands (*in situ*) (Gering et al., 1998), vehicles (carborne) (Aage et al., 2006), airborne (helicopters and fixed wing) (Rawlins et al., 2011) and unmanned aerial vehicle (UAVs) (Okuyama et al., 2008). The height of a detector primarily determines the spatial quality of data given that the field of view (FOV) of the detector will be increased with increasing height (Tyler et al., 1996a). Alongside time and cost restraints this factor is crucial in determining the choice of platform to characterise the underlying spatial distribution of ^{137}Cs contamination.

In situ technologies, utilising highly sensitive HPGe detectors, represent the standard for characterisation of gamma-ray emitting radionuclides (ICRU, 1994). Nonetheless, HPGe detectors generally have low efficiency, require heavy cooling systems and are as a result bulky and not suited for mapping large areas in high spatial resolution. Therefore portable systems, known as mobile gamma-ray spectrometry, tend to use more robust sodium iodide (NaI:Tl) detectors with larger detection volumes (and hence efficiency) in order to improve statistical accuracy (Tyler, 2008). Airborne survey systems as an example can carry hundreds of kilos of NaI:Tl providing very high detection efficiencies that are ideal to rapidly characterise ^{137}Cs contamination on a national scale. However, such surveys come at considerable cost and for safety reasons tend to be conducted at altitudes above 100 m resulting in a large FOV, making resolution of localised contamination difficult. Carborne

systems on the other hand can provide a higher spatial quality of data for significantly less cost whilst still being able to carry significant detection volumes, such surveys tending to be restricted to roads or open fields. UAVs offer enormous potential in the field of gamma-ray spectrometry, however current affordable technologies cannot provide the payloads to carry detectors with sufficient detection efficiency, for long enough periods, to characterise large contaminated areas in high spatial resolution (Martin et al., 2016).

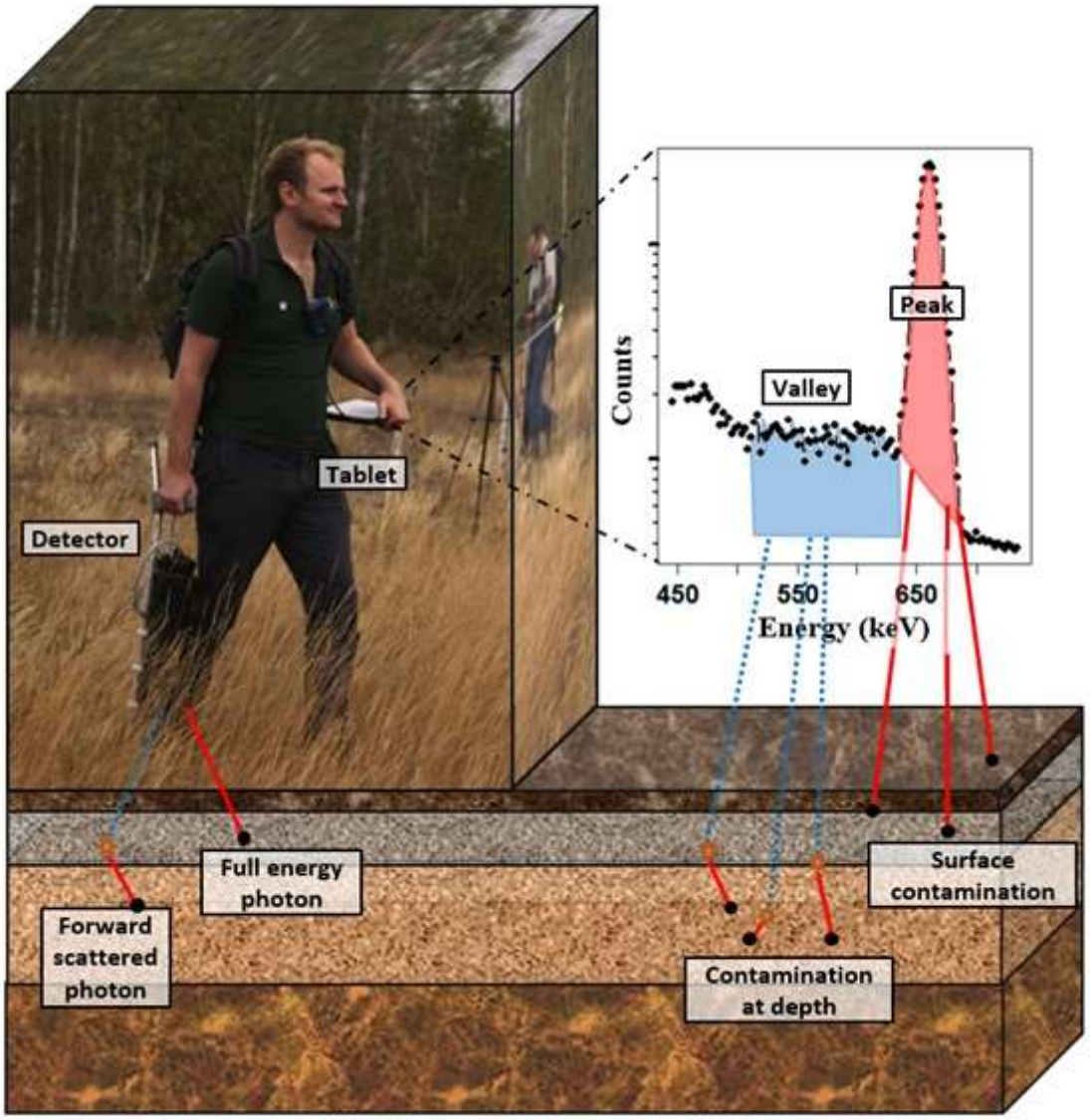

Figure 1. Photograph of a handheld detection system alongside a schematic representation of the peak to valley ratio methodology used to account for burial depth of contamination

Lightweight detection systems originally designed for nuclear security missions are now commonly being implemented in the field as backpack or handheld devices (Figure 1) to characterise ^{137}Cs in relatively heavily contaminated environments (Cresswell et al., 2013; Kock and Samuelsson, 2011; Nilsson et al., 2014; Plamboeck et al., 2006; Sanderson et al., 2013). Typically, a large number of georeferenced spectra are taken during a survey and, conventionally, the count rate in the full energy peak is used to determine the amount of ^{137}Cs contamination in the soil. However, large uncertainties in inventory estimates (Bq m^{-2}) can be encountered when significant spatial heterogeneities in burial depth are encountered. Recently, Varley et al., (2017) demonstrated that through the use of the peak-to-valley ratio (PVR) improved inventory estimates could be made for aged Chernobyl deposits in Belarus. The benefit of utilising the PVR to account for burial depth was first realised by Zombori et al. (1992) and has since been used widely to estimate the burial depth of ^{137}Cs (Feng et al., 2012; Gering et al., 2002, 1998; Kastlander and Bargholtz, 2005; Tyler, 2004). In essence, the PVR is the ratio of the full energy photopeak and the forward scattered photons (Figure 1). Forward scattered photons are those photons that have lost a small amount of energy on transition out of the soil and are represented by the "valley" region of the gamma spectrum that may be observed between the full energy photopeak at 662 keV and the Compton edge occurring at 480 keV. The greater the depth within the soil at which the photon originates, the more probable it is that the photon will undergo forward scattering and generate a count within the valley region of the spectrum. This leads to an increase of the valley "height" and a concomitant decrease in the PVR.

Following the calibration and validation work of assessing the PVR method for mobile handheld gamma spectrometry (Varley et al., 2017) it was apparent that one calibration site exhibited a systematic change in the deposited ^{137}Cs activity and depth distribution towards a tributary of the Pripyat River. The primary aim was to follow up on this observation and to complete a high resolution (<1 m) mobile gamma spectrometry survey across the flood plain to characterise and explain the systematic distribution in a landscape that had been highly impacted by the 1986 Chernobyl accident and that had hitherto been considered to be highly heterogenous with regards to the ^{137}Cs distribution.

Large areas of the watershed of the Pripyat River, the main watercourse of the impacted region and including feeder streams, lakes, marshes and drainages, are within the 30-km exclusion zone that was ultimately imposed around the ChNPP. Since the accident, high

concentrations of radionuclides have been observed within stagnant and slow moving bodies of water associated with the Pripyat River. Such radionuclides accumulate primarily in relation to sediments although accumulations of contaminants can also be observed within the water itself and associated biota (Gudkov et al., 2010). Floodplains have been shown to represent relatively complex post-depositional environments (Golosov et al., 2013; Iwasaki et al., 2015) due to the influence of flood events on a number of processes that govern the environmental behaviour of ^{137}Cs and the contaminated areas of Belarus and Ukraine also bear witness to this complexity (Burrough et al., 1999a; Kagan and Kadatsky, 1996; Zhukova et al., 1997). In this context, it is likely that the systematic mapping of the distribution of ^{137}Cs using handheld mobile gamma spectrometry within the watershed of the Pripyat River in the Polessie State Radioecology Reserve (PSRER), will reveal a complex redistribution of deposited ^{137}Cs at a scale that is likely to be overlooked by conventional sampling, in situ, mobile or airborne gamma spectrometry due to the limitations of sampling or measurement resolution.

2. Methodology

2.1. The Study Site

The selected site (centred at approximately N 51º31′45.2″, E 029º56′07.5″) was known to be periodically inundated given that it lay in a low-lying floodplain within the drainage system of the Pripyat River. Lying some 19 km from the Chernobyl Plant the site had moderate dose rates ranging from 0.1 to 0.5 µSv/h recorded at 1 m in height and contamination densities of ^{137}Cs, ^{90}Sr and ^{241}Am of the order of 1.2 MBq/m^2, 0.2 MBq/m^2 and 0.032 MBq/m^2, respectively. The soils at the site consist primarily of soddy gleys and peat soils of varying density and being better drained at the elevated locations of the site. Vegetation at the site consisted primarily of grasses and mosses, with emergent and submergent macrophytes at lower elevations and near water with some sparse stands of low trees and bushes at the higher elevations.

2.2. Soil sampling and measurement

Soil samples along a transect of approximately 120 m were taken using a steel cylindrical corer (4 cm diameter, 20 cm depth). The transect was selected such that the main features of the site, with respect to potential redistribution of ^{137}Cs, were accounted for. Cores were divided into 2 cm increments. Overlying vegetation and humus was removed prior to sectioning. Soil samples were prepared for radioanalytical measurements by air drying and homogenization followed by mixing and sieving (2 mm aperture). After weighing, a subsample was transferred to an analytical geometry for counting. A HPGe (Canberra, Be5030, carbon window, 50% rel. eff.) detector was used for ^{137}Cs determination. Count times varied from 6000 to 80000 sec. Statistical uncertainties for the photo peak of ^{137}Cs were less than 5 %.

2.3. In situ Gamma Spectrometry

The survey was conducted over the course of a day by two NaI:Tl detectors, a 76 × 76 mm NaI:Tl and a 51 × 51 mm, by two operators. Each detector was connected to an Ortec digiBase recording a 1024 channel spectral per second using Ortec's Maestro software (ORTEC, 2005). GPS coordinates were recorded individually for each spectrum by an SX Blue II differential GPS with an uncertainty of 0.6 m. Spectral measurements and spatial coordinates were combined using software built within the JAVA framework and able to

provide real-time feedback on count rates in specified windows. Maestro's gain stabilisation software was used on the 662 keV peak to avoid significant spectral drift. The detectors were held at a height of about 0.1 m from the ground to reduce the field of view with a traverse speed of approximately 0.5 m s^{-1} being maintained throughout the surveys. To compare the performance of the 51 × 51 mm NaI:Tl against 76 × 76 mm NaI(Tl) concomitant transects for undertaken and tie lines were run perpendicularly across the survey area and compared during the later spatial analysis. Certain sections of the survey area could not be accessed on foot due to the thickness of vegetation and water inundation.

2.4. Detector calibration

Monte Carlo Simulations (MCS) were chosen to derive the relationship between the contamination burial depth and PVR over alternative expensive analytical experiments or complex deterministic equations (Maučec et al., 2009; Stromswold, 1995).Crucially, MCS can depict the variation of PVR with ^{137}Cs depth distribution much more precisely than using a small sample size of soil core data collected in the field (Likar et al., 2004). Furthermore, uncertainties associated with field measurements can be better controlled (Boson et al., 2009) making MCS an important calibration tool in field gamma-ray spectrometry (Cinelli et al., 2016; Clouvas et al., 1998; Maučec et al., 2004; Thummerer and Jacob, 1998; Yip et al., 2015).

In this study, the software package Monte Carlo N-Particle 5 code (MCNP5) was used to obtain spectral responses in order to derive PVR values for appropriate depth distribution (Briesmeister, 1993). To ensure that each depth distribution could be adequately modelled, disk-shaped source descriptions measuring 10 mm thick were simulated down to a depth of 70 g cm^{-3} (Varley et al., 2017). In this manner the PVR could be defined with higher depth resolution and facilitated improved counting statistics as the maximum particle number in MCNP5 (2×10^{-9}) could be run for each simulation, thereby effectively increasing the source density without repeated random number sampling (Hendriks et al., 2002). Although contributing a relatively small number of counts to the detector, the natural radioelements were also modelled in MCNP5 as they were deemed to contribute to the valley region (Varley et al., 2017). Resultantly, source descriptions for ^{40}K and the ^{238}U and ^{232}Th series were also provided to MCNP5 in separate simulations and were assumed to be uniform (Thummerer and Jacob, 1998). Only the main components of each detector were used in

models encompassing the active volume of the detector (NaI:Tl; density 3.51 g cm^{-3}), the aluminium outer canning, the outer casing and the glass window of the photomultiplier tube and the PVC protective outer casing. Detector geometries that were validated in early studies were utilised: 51 × 51 mm (Varley et al., 2015) and 76 × 76 mm (Varley et al., 2017). The codes used to derive these models have been validated using concrete calibration pads (Grasty et al., 1991). The F8 tally implemented in MCNP5 was used to capture the differential energy spectrum within the active volume of each simulated detector. A Gaussian broadening parameter was applied to simulate the statistical broadening of peaks brought about by the imperfect collection of photons within each detector (Kangas et al., 2008) Additionally, as PVR data was generated using energies that can be considered as being immune to photoelectric effect and backscatter by virtue of their energy (>350 keV), a standard soil composition from Beck et al. (1972) was employed and photons below 350 keV were terminated in each run to save on computer time. Photons were recorded at lower energy than the Compton edge (350-478 keV) as it was first thought that this statistically defined region could be used alongside the valley region (496-584 keV) to improve depth estimates. All nuclide decay data used throughout was obtained from the National Nuclear Data Centre (2013).

2.5. Depth distribution model

For the purpose of the study, the relaxation mass per unit area (β) was utilised (eq 1). This relates the rate by which the surface ^{137}Cs activity (A_0) decreases with mass depth in the form of an exponential decay function (ICRU, 1994). Where (A_m) is the ^{137}Cs activity of the soil in Bq kg^{-1} and ζ is the mass of soil per unit area (g cm^{-2}). The value of β will approach 0 for surface contamination and approach ∞ as the contamination is evenly distributed over the entire column. Mass per unit area was preferred over physical depth (cm) in this discussion as it incorporates density (ρ), facilitating a better approximation of shielding effects and permitting a more accurate estimate of ^{137}Cs inventory (Bq m^{-2}). Using this method, each 10 mm slice of ^{137}Cs source model was weighted according to a specific β and inventory value. The total inventory is calculated by integrating eq 1 between the limits of 0 and 70 g cm^{-2}. Given there was a significant layer of vegetation above the soil surface and surrounding the detector, a thickness of 1 g cm^{-2} of lower level contamination was also included in simulations. Contamination densities encountered at the site in overlaying vegetation, although highly heterogeneous, was found to be approximately 5 % the contamination

density of the upper soil layer. Spectral responses derived using this adopted model generated spectral responses that were far more representative of the scattering conditions found in the field.

$$A_m(\zeta) = A_{m,0}.e^{(-\zeta/\beta)} \quad [1]$$

By adopting this approach, one stipulates that the maximum activity will lie within the first few centimetres of soil near the surface; an observation that has, despite the age of contamination, been noted relatively recently at undisturbed sites within the PSRER (Dowdall et al., 2017). Nonetheless, it must be noted that there is still a high probability of a subsurface maximum, particularly in areas of significant accumulation or in the case where the soil type lends itself to high vertical migration rates as observed elsewhere in Europe for example (Bernhardsson et al., 2015). However, in this case the difference in contamination between surface and subsurface maximum is likely to be so small it will be beyond the detection limits for the PVR method. Moreover, the overall difference between final estimates of inventory will be negligible compared to an estimated high β value as would be anticipated using the exponential model (eq 1). Interestingly, environmental processes in the PSRER differ to the process of accumulation of historic Sellafield-derived ^{137}Cs discharges in saltmarsh sediments off the coast of the United Kingdom, in which considerable subsurface maxima can be encountered (Tyler, 1999; Tyler et al., 1996b).

2.6. Estimating inventory using peak-to-valley ratio

The primary purpose of utilising the PVR is as a correction factor to better estimate inventory, therefore the area under the peak (587-737 keV) and the valley height must be calculated for individual field spectra. As there was going to be a small amount of spectral drift throughout the survey, efforts were made to find the peak centroid by fitting a Gaussian function the maximum of which acted as an updated energy calibration. The background under the peak was estimated using a linear function fitted to the adjacent five channels on either side of the base. The estimated background was then subtracted before fitting of a second Gaussian function and integrating to determine the area. The valley height was determined via subtraction of the area on the high energy side of the peak (740-755 keV) from the valley region (496-584 keV) in a manner described by (Tyler et al., 1996b). The routine described above was performed using the base features of the R statistical package (R

Core Development Team, 2016). Once these values had been derived, a linear model was fitted to MCS values of PVR and calculated calibration coefficients (C) (eq 2). Here, C is defined by taking the ratio of the activity (A) measured in Bq m^{-2} and peak count rate (N_p) (eq 3). To obtain the final activity (A) estimate for a field spectrum, the predicted value of C needs to be multiplied by the number of counts in the full energy peak (N_p).

$$log(C) = C_0 + C_s \cdot (PVR) \quad [2]$$

$$C = A/N_p \quad [3]$$

2.7. Quality assessment and mapping of detector estimates

To assess and compare the quality of individual detector performance, approximately 300 one second count time spectra were taken directly over each of the ten extracted cores sites. The PVR method was then applied to each set of spectra to give some approximation of the accuracy and precision of the method, assessed through the mean and standard deviation, respectively. Final maps were produced by combining predicted β and activity values for all data by using the inverse distance weighting algorithm to produce an interpolated surface (Shepard, 1968).

3. Results and Discussion

3.1. Detector predictions compared to core results

Mean activity (kBq m^{-2}) estimations obtained using 51 × 51 mm and 76 × 76 mm sodium iodide detectors over the top of the ten core positions show good agreement with activity and depth results derived from cores (Figure 2). It should be emphasised that single point comparisons may be influenced by the high scale localised heterogeneity emphasising the differences in the spatial representativeness of a single core against a field gamma spectrometry measurement that have >1000 the sample volume. This occurrence is most apparent at site 2, whereby large standard deviations are seen on results for both detectors. Based on this evidence it could be argued that the similarity between detector estimates, particularly with regards to depth, could signal that this approach is in fact more reliable than single coring estimates. In general, it becomes clear that the higher energy efficiency, demonstrated by the 76 × 76 mm, presented an advantage over the 51 × 51 mm especially at lower count rates, which can be realised by a reduction in the spread (standard deviation) of activity and depth estimates at each site. However, this might not always the case where, for example, at much higher activity sites the 51 × 51 mm detector may be more appropriate for deployment due to the amount of dead-time experienced using the 76 × 76 mm.

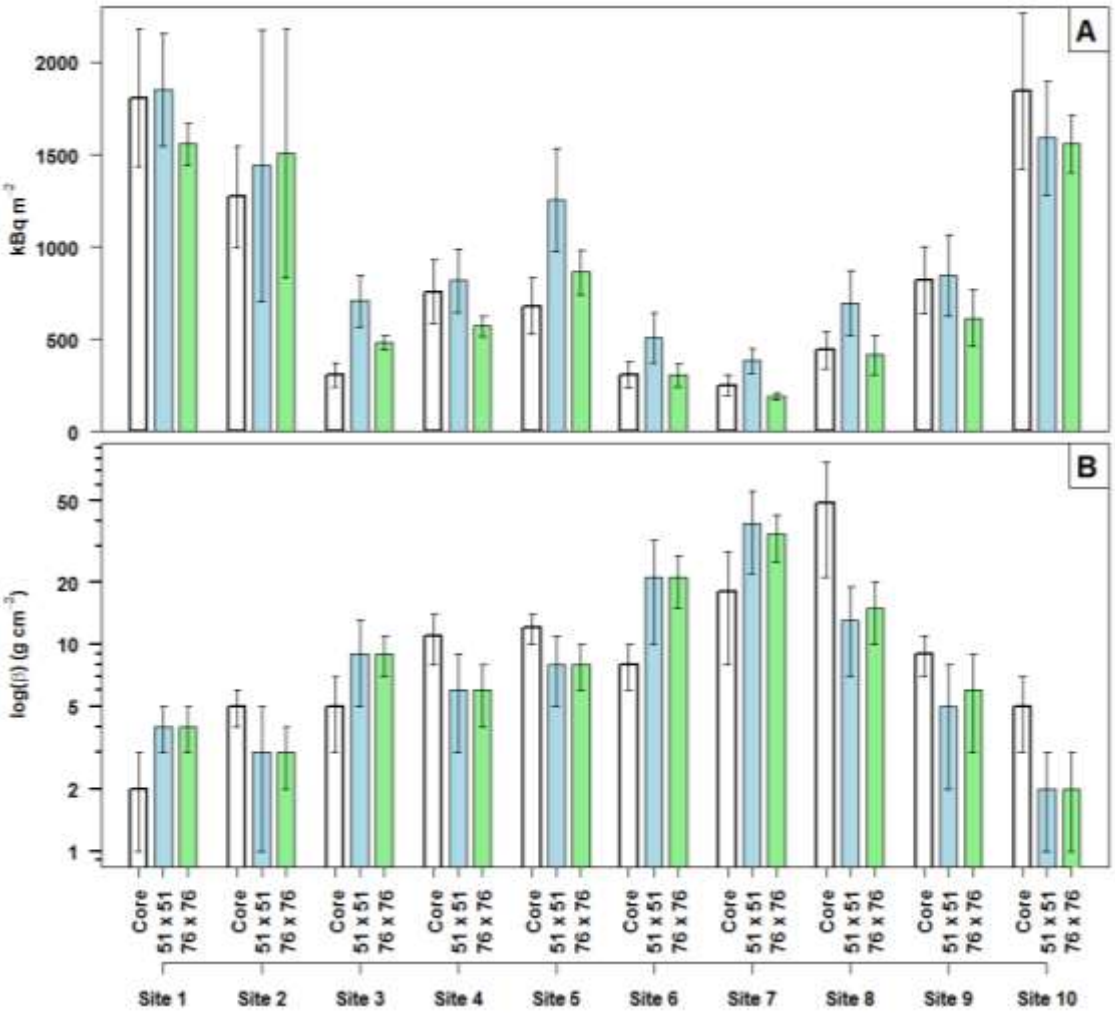

Figure 2. Mean and standard deviations for estimates derived from cores, 51 × 51 mm and 76 × 76 mm for the 10 sites along the transect A) activity (kBq m^{-2}) and B) β (g cm^{-2}).

Overall, results derived using gamma-ray spectrometry provide sufficient evidence that this method is a highly practical option to map the spatial and depth distribution of ^{137}Cs contamination at this site and other sites with similar activities and vertical penetration. Equally, other scintillation instruments, such as lanthanum bromide or cerium bromide, of similar size could also be used effectively (Guss et al., 2010). In identifying ways to reduce uncertainty and thus improve the quality of field data it was concluded that the assumption of an exponential depth distribution must at some stage be reconsidered as this is thought to be the principle cause of error within this study. This fact was highlighted in the fitting of the exponential model to observed core data where large residuals were encountered. For example, R^2 values for cores 7 and 8 were 0.68 and 0.51, respectively. Although for the remaining cores R^2 values were all greater than 0.88. Additionally, vegetation cover and water inundation were revealed to significantly influence instrument response, which would

be hard to characterise by conventional in field calibration, but Monte Carlo simulations present a practical alternative to account for these parameters. It will be the focus of future work to test other distributions in more detail, but within the context of the present study it was accepted that the uncertainty associated with using an exponential distribution would have little influence on final conclusions of contamination distribution.

3.2. Site interpretation

Based on the results of cores taken along the transect, ^{137}Cs is distributed heterogeneously over the extent of the site and is characterised by higher ^{137}Cs inventories, between 1.5 and 2 MBq m^{-2}, exhibited on the elevated areas of the site on both sides of the waterbody (Figure 3). Higher inventories tend to match surface distributions (corresponding to low β values). Conversely, lower ^{137}Cs inventories are primarily confined to the depressions along the transect and correspond reasonably well with areas affected by the rise and fall of the water level in the two bodies of water present; this can be seen in cores 3, 6, 7 and 8. Furthermore, the soils in the associated deeper sections appear to exhibit markedly more pronounced penetration of the contaminant down the soil column. Noticeable subsurface maxima can be observed in cores 7, 8 and 9 (Figure 2). This general observation is, at first consideration, perhaps contrary to what may be expected as there is extensive evidence in the literature that periodic flooding often results in enhancement of ^{137}Cs soils levels due to the addition of contaminated sediment following flood deposition (Burrough et al., 1999b), localised redistribution of eroded soils (Golosov et al., 1999) and the fixation of water borne ^{137}Cs in soils (Standring et al., 2002). Here, however, the lower ^{137}Cs inventories associated with topographical depressions at this site may be explained by three factors possibly acting in combination.

Firstly, contamination was known to be heterogeneously deposited especially in areas close to the reactor such as the PSRER (Boulyga et al., 2003). The possibility therefore exists that the depression at the site simply received less ^{137}Cs when deposition occurred. However, this seems relatively unlikely given that the deposition densities on the elevations on both sides of the water exhibit quite similar values (Figure 3). The systematic distribution of activity estimated from handheld devices provides further support to oppose this notion given that other areas within the study area also possess the highest activities on elevated areas at greater distance from the water body (Figure 3).

A second cause may be associated with soil biogeochemistry owing to the significant presence of organic matter contained within the soil. It is well established that ^{137}Cs remains highly mobile in organic soils (Kudelsky et al., 1996; Rigol et al., 2002; Ritchie and McHenry, 1990; Tegen and Dörr, 1996) primarily due to lower clay mineral contents. As a result, saturated organic soils may exhibit a tendency to lose ^{137}Cs due to its higher mobility, which may ultimately result in lower inventories as ^{137}Cs is lost laterally. Crude examination of the cores revealed the presence of more organic material contained within the lower cores, particularly those that were submerged at the time of extraction (cores 6, 7 and 8). The fact that these same cores exhibit greater depth penetration also supports the theory that mobilisation (as well accumulation) has occurred. Similar profiles of contamination on flood plain soils have been demonstrated by Golosov et al., (Golosov et al., 1999). Yet, without comprehensive chemical analysis data available this theory is hard to prove. Nevertheless, accepting that this is the primary driving force behind the spatial distribution at the site is difficult when considering that significant activity and the gradient of depth variation encountered between elevations and depressions (Graphical abstract).

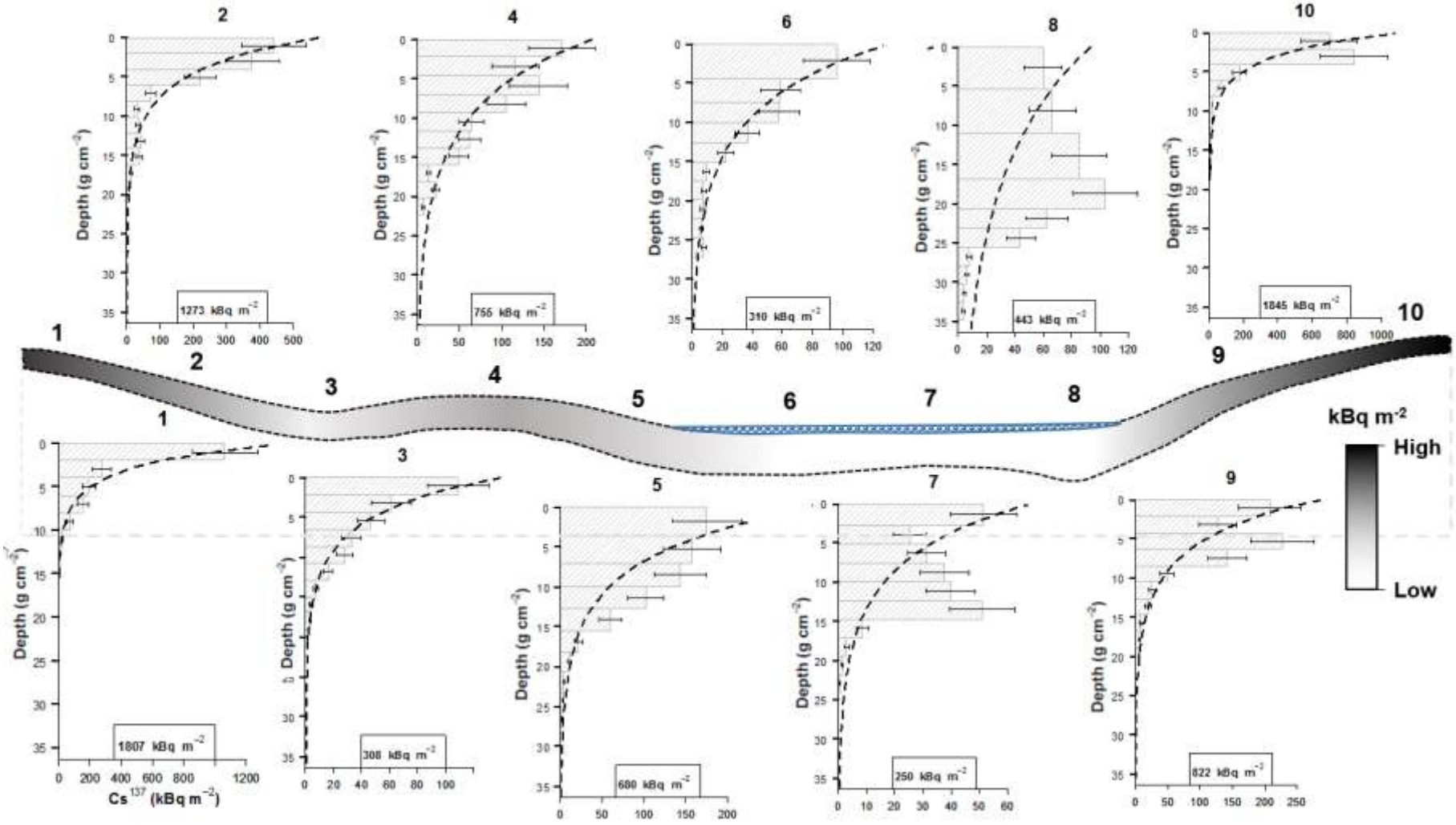

Figure 3. Schematic diagram of estimated elevation alongside depth-activity profiles for cores taken from along the transect

However, the evidence points to a third and perhaps more unusual set of circumstances that may explain the spatial distribution during primary deposition. Regional flooding was known to have taken place during the time of the Chernobyl meltdown brought on by annual snow melt and this can clearly be witnessed over the entire PSRER in 30 m resolution Landsat 5 images taken on the 29th of April 1986 courtesy of the U.S. Geological survey. The pixel resolution of these images is not sufficient enough to directly assess the extent of flooding at the site and it has been difficult to find specific evidence in the literature indicating that this site was flooded in April of 1986. Resultantly, at this stage it cannot be confirmed the extent of flooding at the site, although it was known that other water bodies of the region were in flood at that time (Korobova et al., 2007). Nevertheless, the influence of flood water across the study site can be demonstrated using more recent, considerably higher resolution, satellite imagery taken in autumn 2003 by Googlemaps (Figure 4A) and spring 2008 by Bing imagery (Figure 4B). For example in the Bing images, high flood water can be seen to be inundating much of the flood plain within the main outflow (yellow box), resultantly only the highest elevated areas of the study site (cores 1 and 10) can be seen to be above the water line, with all other core sites between these end members being submerged under flood water (Figure 5B). This evidence, provides the explanation that the areas of lower ^{137}Cs deposition are as a result of flooding at the time of contaminant deposition. Under these conditions, overlying water, potentially containing large amounts of suspended sediment, to which the ^{137}Cs could absorb, delayed it reaching the underlying soil and sediment column and preferentially transporting the ^{137}Cs downstream from the study site. Only elevated areas or those that became exposed during the period of the Chernobyl fire would have received conventional atmospheric deposition (Graphical abstract). Post-accident deposition was then characterised by sediment with similar or lower activity concentrations (cores 7 and 8) that was washed into the area from upstream, gradually burying the ^{137}Cs peak deposition from the time of the accident at a rate that is proportional to the frequency of flood inundation. The rate of accumulation could relate to surface roughness a factor that may heavily be controlled by aquatic and terrestrial vegetation in addition to topography (Figure 3).

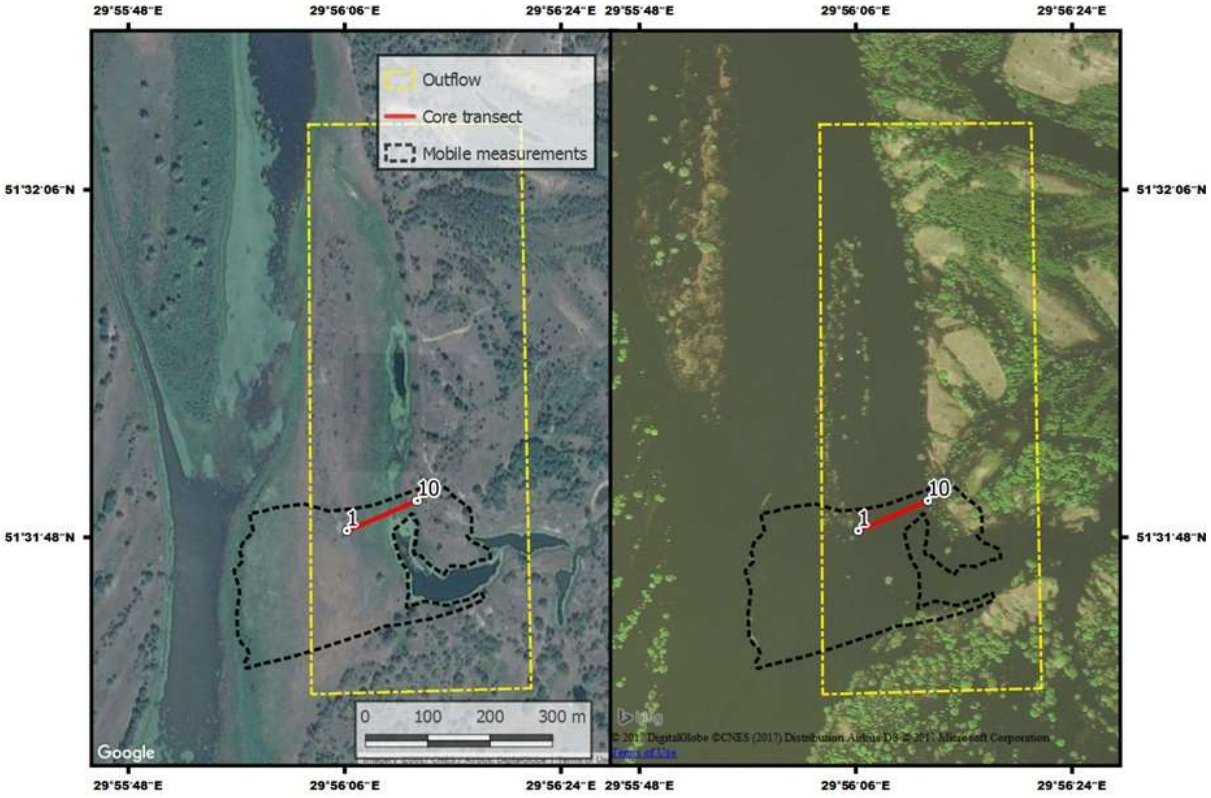

Figure 4. Satellite imagery of the study site in A) Autumn 2003 (Googlemaps) and B) Spring 2008 (Bing imagery). The location of the core transect, the outflow and convex hull of handheld measurements are marked out on the map. The ten samples were collected on the transect marked by the red line.

4. Conclusions

The peak-to-valley ratio method has been successfully applied to data, collected using an inexpensive and robust handheld scintillator, to derive activity and depth estimates of ^{137}Cs contamination within the Polessie State Radioecology Reserve. The study has verified that large areas can be mapped with relatively high accuracy and much faster compared to conventional resource intensive soil sampling approaches. Spatial information gained from the deployment of the handheld gamma spectrometry systems have provided a unique insight into what proved to be a highly complex post-depositional environment, the consequences of which have not been previously explored in the literature. The results have demonstrated that the flooding at the time of the Chernobyl accident can explain systematic variations in deposition across the floodplain and subsequent sediment accumulation is burying the peak ^{137}Cs fallout at a rate that is proportional to the frequency of flooding.

5. Acknowledgements

The mobile gamma-ray spectrometry system was developed by the University of Stirling with funding from the Scottish Environmental Protection Agency with Dr. Paul Dale acting as project manager. Extended gratitude must be given to the staff of the Polessie State Radioecology Reserve for site organisation and transport and Ms. Elena Almås for her impeccable translational skills.

6. References

Aage, H.K., Korsbech, U., Bargholz, K., Hovgaard, J., 2006. Carborne gamma-ray spectrometry. Calibration and applications. Appl. Radiat. Isot. 64, 948–956. doi:http://dx.doi.org/10.1016/j.apradiso.2006.03.013

Beck, H., DeCampo, J., Gogolak, C., 1972. In situ Ge(Li) and NaI(Tl) gamma-ray spectrometry. United States Atomic Energy Commission. doi:10.2172/4599415

Beresford, N.A., Fesenko, S., Konoplev, A., Skuterud, L., Smith, J.T., Voigt, G., 2016. Thirty years after the Chernobyl accident: What lessons have we learnt? J. Environ. Radioact. 157, 77-89.doi:10.1016/j.jenvrad.2016.02.003

Bernhardsson, C., Raaf, C.L., Mattsson, S., 2015. Spatial variability of the dose rate from 137Cs fallout in settlements in Russia and Belarus more than two decades after the Chernobyl accident. J. Environ. Radioact. 149, 144–149. doi:http://dx.doi.org.ezproxy.stir.ac.uk/10.1016/j.jenvrad.2015.07.009

Boson, J., Johansson, L., Rameback, H., Agren, G., 2009. Uncertainty in HPGe detector calibrations for in situ gamma-ray spectrometry. Radiat. Prot. Dosimetry 134, 122–129. doi:10.1093/rpd/ncp079 [doi]

Boulyga, S.F., Zoriy, M., Ketterer, M.E., Sabine Becker, J., 2003. Depth profiling of Pu, 241Am and 137Cs in soils from southern Belarus measured by ICP-MS and alpha α and γ spectrometry. J. Environ. Monit. 5, 661. doi:10.1039/b303621a

Briesmeister, J.F., 1993. MCNP-A general Monte Carlo N-particle transport code. Los Alamos National Laboratory, New Mexico 87545, USA

Burrough, P.A., Van Der Perk, M., Howard, B.J., Prister, B.S., Sansone, U., Voitsekhovitch, O. V, 1999a. Environmental mobility of radiocaesium in the Pripyat catchment, ukraine/belarus. Water. Air. Soil Pollut. 110, 35–55. doi:10.1023/A:1005028729330

Burrough, P.A., Van Der Perk, M., Howard, B.J., Prister, B.S., Sansone, U., Voitsekhovitch, O. V, 1999b. Environmental mobility of radiocaesium in the Pripyat catchment, ukraine/belarus. Water. Air. Soil Pollut. 110, 35–55. doi:10.1023/A:1005028729330

Center, N.N.D., 2013. Nuclear datasheets [WWW Document]. URL http://www.nndc.bnl.gov/ensdf/

Cinelli, G., Tositti, L., Mostacci, D., Baré, J., 2016. Calibration with MCNP of NaI detector for the determination of natural radioactivity levels in the field. J. Environ. Radioact. 155–156, 31–37. doi:10.1016/j.jenvrad.2016.02.009

Clouvas, A., Xanthos, S., Antonopoulos-Domis, M., Silva, J., 1998. Monte Carlo based

562 method for conversion of in-situ gamma ray spectra obtained with a portable Ge detector
563 to an incident photon flux energy distribution. Health Phys. 74, 216–230.
564 doi:10.1097/00004032-199802000-00007
565 Cresswell, A.J., Sanderson, D.C.W., Harrold, M., Kirley, B., Mitchell, C., Weir, A., 2013.
566 Demonstration of lightweight gamma spectrometry systems in urban environments. J.
567 Environ. Radioact. 124, 22–28. doi:10.1016/j.jenvrad.2013.03.006
568 Dowdall, M., Bondar, Y., Skipperud, L., Zabrotski, V., Pettersen, M.N., Selnæs, G., Brown,
569 J.E., 2017. Investigation of the vertical distribution and speciation of 137Cs in soil
570 profiles at burnt and unburnt forest sites in the Belarusian Exclusion Zone. J. Environ.
571 Radioact. 175–176, 60–69. doi:10.1016/j.jenvrad.2017.04.009
572 Feng, T.C., Jia, M.Y., Feng, Y.J., 2012. Method-sensitivity of in-situ gamma spectrometry to
573 determine the depth-distribution of anthropogenic radionuclides in soil. Nucl.
574 Instruments Methods Phys. Res. Sect. A-Accelerators Spectrometers Detect. Assoc.
575 Equip. 661, 26–30. doi:10.1016/j.nima.2011.09.014
576 Gering, F., Hillmann, U., Jacob, P., Fehrenbacher, G., 1998. In situ gamma-spectrometry
577 several years after deposition of radiocesium II. Peak-to-valley method. Radiat. Environ.
578 Biophys. 37, 283–291. doi:10.1007/s004110050130
579 Gering, F., Kiefer, P., Fesenko, S., Voigt, G., 2002. In situ gamma-ray spectrometry in
580 forests: determination of kerma rate in air from 137Cs. J. Environ. Radioact. 61, 75–89.
581 doi:http://dx.doi.org/10.1016/S0265-931X(01)00116-3
582 Golosov, V.N., Belyaev, V.R., Markelov, M. V., 2013. Application of Chernobyl-derived
583 137Cs fallout for sediment redistribution studies: Lessons from European Russia.
584 Hydrol. Process. 27, 781–794. doi:10.1002/hyp.9470
585 Golosov, V.N., Walling, D.E., Panin, A. V., Stukin, E.D., Kvasnikova, E. V., Ivanova, N.N.,
586 1999. The spatial variability of Chernobyl-derived 137Cs inventories in a small
587 agricultural drainage basin in central Russia. Appl. Radiat. Isot. 51, 341–352.
588 doi:10.1016/S0969-8043(99)00050-0
589 Golosov, V.N.V., Walling, D., Kvasnikova, E.V.E., Stukin, E.D., Nikolaev, A.N., Panin, A.
590 V., 2000. Application of a field-portable scintillation detector for studying the
591 distribution of 137Cs inventories in a small basin in Central Russia. J. Environ.
592 Radioact. 48, 79–94. doi:10.1016/S0265-931X(99)00058-2
593 Grasty, R.L., Holman, P.B., Blanchard, Y.B., 1991. Transportable calibration pads for ground
594 and airborne gamma-ray spectrometers. Geological Survey of Canada.
595 Gudkov, D.I., Kuzmenko, M.I., Kireev, S.I., Nazarov, A.B., Shevtsova, N.L., Dzyubenko, E.

596 V, Kaglyan, A.E., 2010. Radioecological Problems of Aquatic Ecosystems of the
597 Chernobyl Exclusion Zone. ISSN Biophys. Radiatsionnaya Biol. Radioekol. 663509,
598 332–339. doi:10.1134/S0006350910020272
599 Guss, P., Reed, M., Yuan, D., Cutler, M., Contreras, C., Beller, D., 2010. Comparison of
600 CeBr(3) with LaBr(3):Ce, LaCl(3):Ce, and NaI:Tl Detectors. Proc. SPIE-The Int. Soc.
601 Opt. Eng. 7805, 78050L–78050L. doi:10.1117/12.862579
602 Hendriks, P.H.G.M., Maucec, M., De Meijer, R.J., Maucec, M., De Meijer, R.J., 2002.
603 MCNP modelling of scintillation-detector gamma-ray spectra from natural
604 radionuclides. Appl. Radiat. Isot. 57, 449–457. doi:10.1016/S0969-8043(02)00118-5
605 ICRU, 1994. Gamm-Ray Spectrometry in the Environmental. International Commission on
606 the Radiation Units and Measurements, 7910 Woodmont Avenue Bethesda, Maryland
607 20814, U.S.A, Maryland 20814, U.S.A.
608 Isaksson, M., Raaf, C., 2017. Environmental Radioactivity and Emergency Preparedness.
609 CRC Press, 6000 Broken Sound Parkway NW, Suite 300, Boca Raton, FL 33487-2742,
610 U.S.A.
611 Iwasaki, T., Nabi, M., Shimizu, Y., Kimura, I., 2015. Computational modeling of 137 Cs
612 contaminant transfer associated with sediment transport in Abukuma River. J. Environ.
613 Radioact. 139, 416–426. doi:10.1016/j.jenvrad.2014.05.012
614 Izrael, Y.A., De Cort, M., Jones, A.R., Nazarov, I.M., Fridman, S.D., Kvasnikova, E. V.,
615 Stukin, E.D., Kelly, G.N., Matveenko, I.I., Pokumeiko, Y.M., Tabatchnyi, L.Y.,
616 Tsaturon, Y., 1996. The atlas of caesium-137 contamination of Europe after the
617 Chernobyl accident. Radiol. consequences Chernobyl Accid. 1–10.
618 Kagan, L.M., Kadatsky, V.B., 1996. Depth migration of chernobyl originated 137Cs and
619 90Sr in soils of Belarus. J. Environ. Radioact. 33, 27–39. doi:10.1016/0265-
620 931X(95)00068-L
621 Kangas, L.J., Keller, P.E., Siciliano, E.R., Kouzes, R.T., Ely, J.H., 2008. The use of artificial
622 neural networks in PVT-based radiation portal monitors. Nucl. Instruments Methods
623 Phys. Res. Sect. A Accel. Spectrometers, Detect. Assoc. Equip. 587, 398-412.
624 doi:10.1016/j.nima.2008.01.065
625 Kastlander, J., Bargholtz, C., 2005. Efficient in situ method to determine radionuclide
626 concentration in soil. Nucl. Instruments Methods Phys. Res. Sect. A-Accelerators
627 Spectrometers Detect. Assoc. Equip. 547, 400–410. doi:10.1016/j.nima.2005.03.143
628 Kock, P., Samuelsson, C., 2011. Comparison of airborne and terrestrial gamma spectrometry
629 measurements - evaluation of three areas in southern Sweden. J. Environ. Radioact. 102,

605–613. doi:10.1016/j.jenvrad.2011.03.010
Konoplev, A., Golosov, V., Wakiyama, Y., Takase, T., Yoschenko, V., Yoshihara, T., Parenyuk, O., Cresswell, A., Ivanov, M., Carradine, M., Nanba, K., Onda, Y., 2017. Natural attenuation of Fukushima-derived radiocesium in soils due to its vertical and lateral migration. J. Environ. Radioact. 186, 23-33. doi:10.1016/j.jenvrad.2017.06.019
Korobova, E., Linnik, V., Chizhikova, N., 2007. The history of the Chernobyl 137 Cs contamination of the flood plain soils and its relation to physical and chemical properties of the soil horizons (a case study). J. Geochem. Expl. 96, 236-255 doi:10.1016/j.gexplo.2007.04.014
Kudelsky, A. V, Smith, J.T., Ovsiannikova, S. V, Hilton, J., 1996. Mobility of Chernobyl-derived137Cs in a peatbog system within the catchment of the Pripyat River, Belarus. Sci. Total Environ. 188, 101–113. doi:10.1016/0048-9697(96)05162-5
Likar, A., Vidmar, T., Lipoglavsek, M., Omahen, G., 2004. Monte Carlo calculation of entire in situ gamma-ray spectra. J. Environ. Radioact. 72, 163–168.
Mabit, L., Dercon, G., 2014. Guidelines for using fallout radionuclides to assess erosion and effectiveness of soil conservation strategies (IAEA-TECDOC-1741), International Atomic Energy Agency. 1400 Vienna, Austria
Martin, P.G., Payton, O.D., Yamashiki, Y., Richards, D.A., Scott, T.B., 2016. High-resolution radiation mapping to investigate FDNPP derived contaminant migration. J. Environ. Radioact. 164, 26–35. doi:http://dx.doi.org/10.1016/j.jenvrad.2016.06.025
Maučec, M., de Meijer, R.J., Rigollet, C., Hendriks, P.H.G.M., Jones, D.G., 2004. Detection of radioactive particles offshore by γ-ray spectrometry Part I: Monte Carlo assessment of detection depth limits. Nucl. Instruments Methods Phys. Res. Sect. A Accel. Spectrometers, Detect. Assoc. Equip. 525, 593–609. doi:10.1016/j.nima.2004.01.074
Maučec, M., Hendriks, P.H.G.M., Limburg, J., de Meijer, R.J., 2009. Determination of correction factors for borehole natural gamma-ray measurements by Monte Carlo simulations. Nucl. Instruments Methods Phys. Res. Sect. A Accel. Spectrometers, Detect. Assoc. Equip. 609, 194–204. doi:http://dx.doi.org/10.1016/j.nima.2009.08.054
Miller, M.L., 2007. Cesium-137 in the Environment: Radioecology and Approaches to Assessment and Management. NCRP Rep. No.154, Cesium-137 Environ. Radioecol. Approaches to Assess. Manag. 151.
Nilsson, J.M.C., Östlund, K., Söderberg, J., Mattsson, S., Rääf, C., 2014. Tests of HPGe- and scintillation-based backpack γ-radiation survey systems. J. Environ. Radioact. 135, 54–62. doi:10.1016/j.jenvrad.2014.03.013

Okuyama, S.-I., Torii, T., Suzuki, A., Shibuya, M., Miyazaki, N., 2008. A Remote Radiation Monitoring System Using an Autonomous Unmanned Helicopter for Nuclear Emergencies A Remote Radiation Monitoring System Using an Autonomous Unmanned Helicopter for Nuclear Emergencies. J. Nucl. Sci. Technol. 45, 5–414. doi:10.1080/00223131.2008.10875877

Penrose, B., Johnson née Payne, K.A., Arkhipov, A., Maksimenko, A., Gaschak, S., Meacham, M.C., Crout, N.J.M., White, P.J., Beresford, N.A., Broadley, M.R., 2016. Inter-cultivar variation in soil-to-plant transfer of radiocaesium and radiostrontium in Brassica oleracea. J. Environ. Radioact. 155, 112–121. doi:10.1016/j.jenvrad.2016.02.020

Plamboeck, A.H., Nylén, T., Ågren, G., 2006. Comparative estimations of 137Cs distribution in a boreal forest in northern Sweden using a traditional sampling approach and a portable NaI detector. J. Environ. Radioact. 90, 100–109. doi:10.1016/j.jenvrad.2006.06.011

Povinec, P.P., Bailly du Bois, P., Kershaw, P.J., Nies, H., Scotto, P., 2003. Temporal and spatial trends in the distribution of 137Cs in surface waters of Northern European Seas: a record of 40 years of investigations. Worldw. Mar. Radioact. Stud. 50, 2785–2801. doi:http://dx.doi.org/10.1016/S0967-0645(03)00148-6

Povinec, P.P., Hirose, K., Aoyama, M., Povinec, P.P., Hirose, K., Aoyama, M., 2013. 5 – Fukushima Radioactivity Impact, in: Fukushima Accident. pp. 131–275. doi:10.1016/B978-0-12-408132-1.00005-X

R Core Development Team, 2016. R: A language and environment for statistical computing. R Foundation for Statistical Computing. ISBN 3-900051-07-0

Rawlins, B.G., Scheib, C., Beamish, D., Webster, R., Tyler, A.N., Young, M.E., 2011. Landscape-scale controls on the spatial distribution of caesium 137: A study based on an airborne geophysical survey across Northern Ireland. Earth Surf. Process. Landforms 36, 158–169. doi:10.1002/esp.2026

Rigol, A., Vidal, M., Rauret, G., 2002. An overview of the effect of organic matter on soil–radiocaesium interaction: implications in root uptake. J. Environ. Radioact. 58, 191–216.

Ritchie, J.C., McHenry, J.R., 1990. Application of Radioactive Fallout Cesium-137 for Measuring Soil Erosion and Sediment Accumulation Rates and Patterns: A Review. J. Environ. Qual. 19, 215–233. doi:10.2134/jeq1990.00472425001900020006x

Sanderson, D., Cresswell, A., Seitz, B., Yamaguchi, K., Takase, T., Kawatsu, K., Suzuki, C., Sasaki, M., 2013. Validated Radiometric Mapping in 2012 of Areas in Japan Affected

by the Fukushima-Daiichi Nuclear Accident. Scottish Universities Environmental Research Centre, University of Glasgow, Scotland doi:10.5525/GLA.RESEARCHDATA.67

Shepard, D., 1968. A two-dimensional interpolation function for irregularly-spaced data, in: Proceedings of the 1968 23rd ACM National Conference. ACM, pp. 517–524.

Standring, W.J.F., Oughton, D.H., Salbu, B., 2002. Potential remobilization of 137Cs, 60Co, 99Tc, and 90Sr from contaminated Mayak sediments in river and estuary environments. Environ. Sci. Technol. 36, 2330–2337. doi:10.1021/es0103187

Stromswold, D.C., 1995. Calibration facilites for borehole and surface environmental radiation measurements. J. Radioanal. Nucl. Chem. 194, 393–401.

Tegen, I., Dörr, H., 1996. Mobilization of cesium in organic rich soils: correlation with production of dissolved organic carbon. Water. Air. Soil Pollut. 88, 133–144. doi:10.1007/BF00157418

Thummerer, S., Jacob, P., 1998. Determination of depth distributions of natural radionuclides with in situ gamma-ray spectrometry. Nucl. Instruments Methods Phys. Res. Sect. A-Accelerators Spectrometers Detect. Assoc. Equip. 416, 161–178. doi:10.1016/S0168-9002(98)00636-6

Tyler, A., 1999. Monitoring anthropogenic radioactivity in salt marsh environments through in situ gamma-ray spectrometry. J. Environ. Radioact. 45, 235-252.

Tyler, A., Sanderson, D., Scott, E., 1996a. Accounting for spatial variability and fields of view in environmental gamma ray spectrometry. J. Environ. Radioact. 33, 213-235.

Tyler, A., Sanderson, D., Scott, E., 1996b. Estimating and accounting for 137 Cs source burial through in-situ gamma spectrometry in salt marsh environments. J. Environ. Radioact. 33, 195-212.

Tyler, A.N., 2008. In situ and airborne gamma-ray spectrometry, in: Radioactivity in the Environment, Analysis of Environmental Radionuclides. Elsevier, pp. 407–448. doi:10.1016/S1569-4860(07)11013-5

Tyler, A.N., 2004. High accuracy in situ radiometric mapping. J. Environ. Radioact. 72, 195–202. doi:10.1016/S0265-931X(03)00202-9

Varley, A., Tyler, A., Dowdall, M., Bondar, Y., Zabrotski, V., 2017. An in situ method for the high resolution mapping of 137 Cs and estimation of vertical depth penetration in a highly contaminated environment. Sci. Total Environ. 605–606, 957–966. doi:10.1016/j.scitotenv.2017.06.067

Varley, A., Tyler, A., Smith, L., Dale, P., 2015. Development of a neural network approach

to characterise 226Ra contamination at legacy sites using gamma-ray spectra taken from boreholes. J. Environ. Radioact. 140, 130–140. doi:http://dx.doi.org/10.1016/j.jenvrad.2014.11.011

Yip, M., Saripan, M., Wells, K., Bradley, D., 2015. Monte Carlo Simulations for the Detection of Buried Objects Using Single Sided Backscattered Radiation. PLoS One.

Zhukova, O.M., Matveenko, I.I., Myshkina, N.K., Sharovarov, G.A., Shiryaeva, N.M., 1997. Formation and dynamics of propogation of radioactive contamination in rivers of Belarus after the Chernobyl nuclear accident. J. Eng. Phys. Thermophysics Inzhenerno-Fizicheskii Zhurnal 70, 73–80.

Zombori, P., Nemeth, I., Andrasi, A., Lettner, H., 1992. In-situ gamma-spectrometric measurement of the contamination in some selected settlements of Byelorussia (BSSR), Ukraine (UkrSSR) and the Russian Federation (RSFSR). J. Environ. Radioact. 17, 97–106. doi:http://dx.doi.org/10.1016/0265-931X(92)90019-P